First-principles study of rare gas incorporation in titanium nitride

R. Bès,[1,*] Y. Pipon,[1,†] N. Millard-Pinard,[1] S. Gavarini,[1] and M. Freyss[2]
[1]*Université de Lyon, Université Lyon 1, CNRS/IN2P3, UMR5822, IPNL, F-69622 Lyon, France*
[2]*CEA, DEN, DEC/SESC/LLCC, Centre de Cadarache, 13108 Saint-Paul-lez-Durance, France*
(Received 31 July 2012; published 8 January 2013)

First-principles calculations have been carried out to study the incorporation of rare gas atoms, with a focus on xenon, in titanium nitride. The density functional theory–generalized gradient approximation method has been used to calculate the formation energy of several point defects (vacancies, interstitials, divacancies, Frenkel pairs) and then the incorporation energies of rare gases in these defects. The main results show that nitrogen vacancies are the most probable defects as well as the Schottky defects. Incorporation energy calculations suggest that the most favorable Xe host sites involve vacancies as the Schottky defect with vacancies located on the edge of the cubic lattice.

DOI: 10.1103/PhysRevB.87.024104 PACS number(s): 61.72.J−, 61.72.Bb, 61.72.S−, 81.05.Je

I. INTRODUCTION

In recent years, titanium nitride (TiN) has been the subject of considerable experimental and theoretical attention. TiN's wide range of application covers various domains from decorative to electronic and nuclear applications.

TiN has a goldlike appearance due to its optical spectrum similarity with that of gold. So, it is commonly deposited as a protective and decorative layer in jewelery.[1–4] TiN could also be used as material for solar control coatings in architecture, renewable energy, and automotive glass.[5–10] TiN is a hard refractory material with rocksalt structure. Its hardness, near that of diamond, has led to several applications in wear-resistant coating as cutting tools[11–13] and superhard material.[14–16] Its good biocompatibility makes it useful in clinical dentistry[17–19] and biological implants.[20–23]

In the microelectronics industry, TiN is widely used as a contact material[24,25] and as a diffusion barrier in electronic devices.[26–33] In this context, thin TiN films are generally obtained using physical vapor deposition (PVD) processes. Most of these reactive processes employ low-energy ion irradiation to modify thin-film microstructure and composition during growth. However, ion irradiation can also drive point defect generation, incorporation of the noble gas (He, Ar, or Kr) that is present in the PVD atmosphere, and excess nitrogen composition.[34] As a consequence, gas bubble precipitation during growth of TiN films could degrade the awaited properties of the film.

In the context of the generation IV project concerning future nuclear reactors operating at high temperature, such as the gas-cooled fast reactor (GFR), TiN is an interesting candidate as cladding for advanced nuclear fuel[35] due to its adequate properties (mechanical and thermal stability, resistance at high temperature and under irradiation).[36,37] The most likely fissile particle types of these advanced fuels are (U,Pu)C and (U,Pu)N due to the combination of high thermal conductivity and high actinide density. Chemical compatibility issues favor the use of a nitride coating system (TiN or ZrN) for mixed nitride kernels and a carbide coating system (SiC, TiC, or ZrC) for mixed carbide kernels.

In the case of GFRs, coolant gas (He) infusion, minor actinide decays (He), and gaseous fission products (Kr and Xe) implantation could degrade inert matrix performances during the in-pile process.

As can be seen from the wide range of applications of TiN, the behavior of rare gases and their interaction with point defects, especially created under irradiation, is a common problem. Nevertheless, to our knowledge, few experimental studies can be found in the literature concerning rare gas behavior in this refractory material.

In 1990, Weber *et al.*[38] estimated the critical concentration of xenon precipitation in TiN films to be lower than 0.5 at. %. In 1992, Perry *et al.*[39] studied the modification of the lattice parameter and the residual stress due to Ar and Kr implantation in TiN films. They showed that for concentration lower than 1 at. %, Kr and Ar atoms are certainly located in lattice vacancies or associated with lattice vacancies. No information has been given about the type of vacancies involved in this behavior. Formation of Kr and Ar bubbles have also been observed in implanted samples for concentration higher than 4 at. %. As a consequence, the solubility limit of Ar and Kr probably ranges between 1 and 4 at. %. More recently, in a review paper on nitride films, Hultman[34] discussed Ar diffusion in TiN. It was found that up to 1 at. % of Ar atoms can be trapped in films during growth of TiN films. This amount of Ar is mostly (approximatively 97%) contained in the lattice, implying that Ar atoms may probably be associated with lattice defects.

Extensive experimental studies[40–43] were performed on the thermal behavior of implanted Xe in sintered TiN. The Xe diffusion coefficient and transport velocity towards the surface under annealing at high temperature (between 1573 to 1873 K) have been measured. Intragranular square-shaped bubbles have been observed for Xe concentration lower than 0.4 at. %. These bubbles seem to migrate at high temperature, suggesting a role played by lattice vacancies created either during the implantation process or during the annealing treatments.

The driving mechanism responsible for bubble migration in sintered TiN is still not well understood. As a consequence, further studies are needed to determine the nature of defects and the incorporation sites involved in the rare gas behavior in titanium nitride. Indeed, vacancies constitute possible traps for impurities such as rare gases.

A possible key to obtain this information is the use of first-principles calculations. Using first-principles calculations, Tsetseris *et al.*[44] showed that He and Ar are preferentially trapped in a N vacancy site.

The aim of the present work is to determine the most favorable incorporation site for the inert gas atoms with a focus on Xe by using first-principles density functional theory calculations. This approach is a complementary understanding of the previous experimental and calculated results on the behavior of inert gas atoms in TiN. In Secs. II and III, we describe the methodology. Sections IV and V give, respectively, the obtained results on the structure and energetics of point defects and inert gas incorporation in TiN.

II. CALCULATION METHODS

All of these calculations were performed within the framework of density functional theory (DFT) and more particularly with the first-principles projector augmented wave (PAW)[45] method as implemented in the VASP code.[46] The exchange-correlation interaction was estimated using the Perdew-Wang 91 generalized gradient approximation (PW91-GGA).[47] The energy cutoff (E_c) of the plane-wave basis set was chosen to be 800 eV. TiN crystal has the rocksalt structure (space group $225/Fm\bar{3}m$).[37] The results presented in the following sections are mainly based on $2 \times 2 \times 2$ supercells with 32 Ti and 32 N atoms for a 64-atom supercell without any defect. To ensure convergence of the results, calculations were also performed using $3 \times 3 \times 3$ supercells with 108 Ti and 108 N atoms on the defect-free 216-atom titanium nitride crystal. A $6 \times 6 \times 6$ Monkhorst-Pack k-point mesh[48] was used to sample the irreducible Brillouin zone of the 64-atom supercell. Such parameters are sufficient to get the defect-formation and the rare-gas incorporation energies converged to less than 50 meV. In all the calculations, the atomic positions are relaxed until the maximum residual forces are below 10^{-5} eV Å^{-1}. The spin polarization was neglected due to the absence of magnetism that was evidenced in preliminary calculations on bulk properties of TiN (see Sec. III C).

III. BULK PROPERTIES OF TiN

To ensure that the calculated TiN crystal reproduced as well as possible the properties of TiN, bulk properties of titanium nitride such as the equilibrium lattice parameter, the bulk modulus, and the formation energy were calculated and compared to literature data. These results are reported here.

A. Bulk modulus and equilibrium lattice parameter

The bulk modulus and equilibrium lattice parameter of TiN are deduced from the fitting of the calculated total energy as a function of the lattice parameter by the Birch-Murnaghan isothermal equation of state.[49] Table I gives the results obtained, together with the literature data (experiments and calculations).

As it can be seen, the bulk modulus of TiN is underestimated by 5% and the equilibrium lattice parameter is overestimated by 0.3% compared to the experimental value. These results are in fair agreement with experimental values and in the same order of magnitude as previous calculations.[50–53]

TABLE I. Calculated equilibrium lattice parameter a and bulk modulus B_0 of TiN. Comparison with literature data is also reported.

a (nm)	B_0 (GPa)	Method
0.4253	274	PAW-GGA, VASP code (this work)
0.4236		PAW-GGA, VASP code[50]
0.4247	270	PAW-GGA, SIESTA code[51]
0.4250	270	PWPP-GGA,[a] DACAPO code[52]
0.4236	282	Ultrasoft-PWPP-GGA, CASTEP code[53]
0.4240	288	Experiment[51]

[a]PWPP, plane-wave pseudopotential.

Consequently, these bulk properties are well reproduced by our calculation.

B. Enthalpy of formation

The formation energy of TiN, $E_{\text{form}}^{\text{TiN}}$ is obtained combining the cohesive energies of TiN and its constitutive elements. Here the metallic α-Ti (space group $194/P6_3/mmc$, stable below 882°C)[37] and the isolated molecule of N_2 have been chosen as the constitutive elements due to the experimental conditions of the usual TiN powder synthesis process which follows the reaction $\alpha\text{-Ti}_{(s)} + \frac{1}{2}\text{N}_{2(g)} \rightleftharpoons \text{TiN}_{(s)}$. After atomic position relaxation, the equilibrium lattice parameters of α-Ti are in fair agreement with experimental values with a relative error less than 0.5%. The N_2 molecule is obtained with a distance between both N atoms equal to 1.11 Å and a binding energy of 10.76 eV. These values are qualitatively well comparable with the respective experimental values of 1.10 Å and 9.80 eV.[54] In crystalline solids, the formation energy represents the major part of the enthalpy of formation, ΔH_{form}. Indeed, the additional contributions, i.e., the lattice and electronic excitation energies, are typically less than 2% of the enthalpy of formation at the ambient temperature. They can be neglected considering the experimental and theoretical accuracy in its determination. Assuming this, it yields the formation energies per atom, ΔH_{form}, calculated by Eq. (1):

$$\Delta H_{\text{form}} \simeq E_{\text{form}}^{\text{TiN}} = \frac{E_{\text{tot}} - N_{\text{Ti}} E_{\text{Ti}} - N_{\text{N}} E_{\text{N}}}{N_{\text{Ti}} + N_{\text{N}}} \qquad (1)$$

This expression requires the first-principles calculations of the total energy for the TiN compound, E_{tot}, the α-Ti crystal energy per atom, E_{Ti}, and the isolated molecule N_2 energy per atom, E_{N}. N_{Ti} and N_{N} are respectively the total numbers of titanium and nitrogen atoms involved in the total energy E_{tot} calculation for the TiN compound. The value obtained is 1.751 eV atom^{-1} and is in good agreement with the experimental 1.750 eV atom^{-1}.[37]

C. Electron density of states

In Fig. 1 are shown the titanium and nitrogen orbital projected densities of states (DOS) of the bulk TiN. Spin-up and spin-down DOS have identical features, which indicates that no magnetic moment is present in TiN. As a consequence, the spin polarization is neglected in the following point defects stability and rare gases incorporation calculations. One can also notice the important contribution of the 3d Ti orbital on

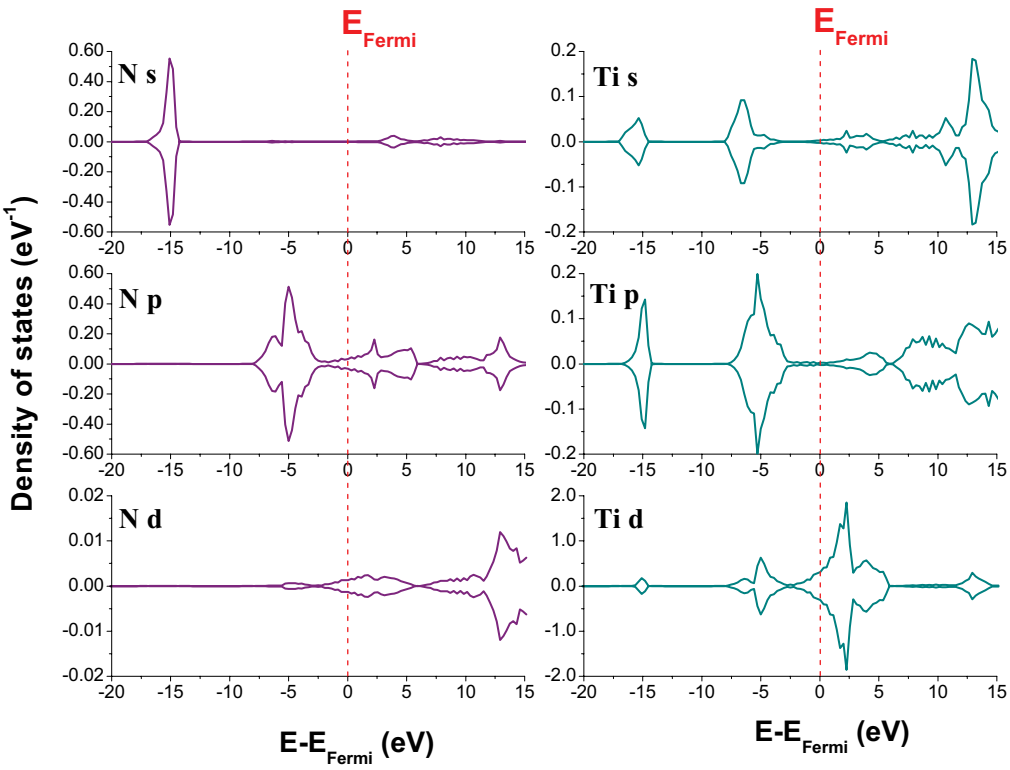

FIG. 1. (Color online) Local electronic density of states of s, p, and d electronic shells obtained in spin-polarized calculations. For the sake of clarity, the spin-down densities have been multiplied by -1.

the conducting band at and above the Fermi level confirming the metallic properties of TiN. There is also a strong $2p$ N and $3d$ Ti hybridization in the valence band. These results are in fair agreement with the previous studies by Guemmaz *et al.*[55,56] and Tsetseris *et al.*[57]

IV. POINT DEFECTS STABILITY IN TiN

A. Formation energy of point defect

The formation energy $E_f(m_X V_X, n_X I_X)$ (where $X =$ Ti or N) of the defect composed by m_X vacancies (V_X) and n_X interstitials (I_X), is calculated with the following expression:

$$E_f(m_X V_X, n_X I_X) = E[\mathrm{TiN} + \mathrm{defect}] + \sum_{X=\mathrm{Ti,N}} (m_X - n_X) E[X] - E[\mathrm{TiN}], \quad (2)$$

where $E[\mathrm{TiN}]$ is the energy of the defect-free TiN supercell and $E[\mathrm{TiN} + \mathrm{defect}]$ is the energy of the supercell containing the defect. $E[X]$ (where $X =$ Ti or N) is the energy per atom of each chemical species Ti and N in its reference state involved in each vacancy or interstitial composing the final defect. These energies require the knowledge of an arbitrary reference state which has been chosen, as mentioned before, as the ground-state crystalline phase of titanium, i.e., α-Ti, and the isolated nitrogen molecule N_2 in vacuum.

One can keep in mind that in this expression the temperature dependence is not taken into account. To do so, one has to calculate the free energy of the defect formation. The temperature dependence on the formation free energy of defects could be estimated following the example of Evarestov *et al.*[58] for oxygen vacancy formation in $SrTiO_3$, or the approach by Mastrikov *et al.*,[59] Johnston *et al.*,[60] and Heifets *et al.*[61,62] for oxygen interactions with $LaMnO_3$, $BaZrO_3$, and $SrTiO_3$ surfaces. Evarestov *et al.* found that the solid-phase phonon contribution to the defect formation free energy remains small (less than 5%) up to 1000 K and can thus be neglected. Instead, most of the temperature dependence of the formation energy of point defects comes from the temperature dependence of the chemical potential of the nitrogen molecule in the gas phase. Evarestov *et al.* determined this oxygen chemical potential by calculation of the free energy of the gas-phase oxygen molecule, including vibrational properties of the molecule, and with no use of experimental data. Here, the vibrational properties of the N_2 molecule have not been calculated, but the N_2 chemical potential was assessed by the temperature dependence of the N_2 gas Gibbs free energy obtained using thermodynamical data.[63] According to this approach, the N_2 chemical potential was found to decrease compared to 0 K, by 0.15 eV at ambient temperature and 0.31 eV at 600 K. Consequently, the nitrogen defect formation free energies would vary by the same amount at the respective temperatures, compared to the formation energies calculated at 0 K. So, the formation energy of a nitrogen vacancy is reduced by 0.15 eV and the formation energy of a nitrogen interstitial is increased by 0.15 eV at room temperature.

B. Single point defects

Table II gives the calculated formation energies of the studied single point defects. All of these results are described and discussed in details in the following sections.

TABLE II. Calculated formation energies of the single point defects in the TiN crystal. The values of monovacancies (V_N and V_{Ti}), self-interstitials (I_N and I_{Ti}), first neighboring Frenkel pairs (FP_{Ti}^{first} and FP_N^{first}), first and second neighboring mixed divacancies [V_{TiN}(first) and V_{TiN}(second)] and split aligned (110) nitrogen interstitial [$D_N^N(110)$] are given and compared with literature data.

Reference	V_N (eV)	V_{Ti} (eV)	I_N (eV)	I_{Ti} (eV)	FP_{Ti}^{first} or FP_N^{first}
This work	2.41	3.28	4.93	8.28	Recombination
Ref. 51	[−0.47;3.38]	[0.2;4.19]			
Ref. 57	2.41		5.46		
Reference	V_{TiN}(first) (eV)	V_{TiN}(second) (eV)	V_{TiN}(first)[a] (eV)	V_{TiN}(second)[a] (eV)	$D_N^N(110)$ (eV)
This work	5.63	5.80	5.28	5.32	4.33
Ref. 57					4.6

[a]Calculations performed with a 216-atom supercell.

The atomic displacements δR, i.e., changes in atomic separation distance, due to the presence of Ti or N vacancies and interstitials after structural optimization of the unit cells are given in Table III. The changes in atomic separation are deduced from the position of atomic shells surrounding the considered lattice site, according to the separation distance between this site and the surrounding atoms in the perfect TiN lattice. For example in the perfect crystal, taking a titanium (nitrogen) site, the nearest-neighbor shell is 2.13 Å away from the reference site and contains 6 N (Ti) atoms. The second neighboring shell is located 3.01 Å away from the reference site and consists of 12 Ti (N) atoms. In the case of the interstitial tetrahedral site, the nearest-neighbor shell contains 4 Ti and 4 N atoms at a distance of 1.84 Å. The next-nearest-neighbor shell is 3.33 Å away from the tetrahedral site and contains 12 Ti and 12 N atoms.

1. Vacancies

As it can be seen in Table II, the formation of the nitrogen and titanium vacancies (V_N and V_{Ti}, respectively) is less expensive than for other defects by more than 1 eV. These values reveal that vacancies are the most probable defect considering all of the defects studied here. Moreover, these results are in fair agreement with the values obtained by Tsetseris *et al.*[50] and Carara *et al.*[51]

The formation of V_N costs 0.87 eV less than the formation of V_{Ti}. Therefore, we can assume that nitrogen vacancies are the most probable defects in TiN. This assumption is confirmed by the fact that, experimentally, TiN is known to be stable for a large range of stoichiometry, from 0.6 to 1.2.[34]

As already observed by Jhi *et al.*[64,65] and Tsetseris *et al.*,[50,57] a nitrogen vacancy V_N induces a small relaxation in the surrounding TiN matrix. The distance between neighboring Ti atoms and the V_N site increases from 2.13 to 2.23 Å. By contrast, the second shell distance δR_{second} around the vacancy contracts only ∼0.01 Å. Concerning the titanium vacancy V_{Ti}, a structural relaxation is also observed. The first neighboring shell distance δR_{first} increases by 0.04 Å. The second shell of Ti atoms contracts its bonding distance from 3.01 to 2.94 Å. As already mentioned by Carara *et al.*,[51] the presence of vacancies leads to structural rearrangements of the atomic position up to the second neighboring shell only. Indeed, the breaking of bonds results in the reduction of interatomic distances between the first and second neighboring shells.

TABLE III. Atomic displacements of the first shell(s), δR, due to the presence of point defects in TiN. Negative (positive) values indicate a decrease (increase) of the interatomic distances.

Species	δR_{first} (Å)	δR_{second} (Å)
V_N	+0.1 (Ti)	−0.01 (N)
V_{Ti}	+0.04 (N)	−0.07 (Ti)
I_N	+0.3 (Ti)/+0.04 (N)	+0.03 (Ti)/+0.02 (N)
I_{Ti}	+0.4 (Ti)/+0.06 (N)	+0.06 (Ti)/+0.06 (N)

2. Interstitials

Here, the nitrogen and titanium interstitials (I_N and I_{Ti} in tetrahedral position) are discussed. A split (110) aligned nitrogen interstitial for which the extra N atom forms a stretched N-N bonding with an N atom of the surrounding matrix, usually named dumbbell and denoted $D_N^N(110)$, is also considered. Here, the dimer N-N points along the (110) direction as it can be seen in Fig. 2(a).

In Table II, one can first note that the formation energy of the nitrogen interstitial in both tetrahedral and split-aligned (110) sites [I_N and $D_N^N(110)$, respectively] is less expensive than a titanium interstitial I_{Ti} (tetrahedral site). Moreover, according to Table III, introducing a titanium atom in a tetrahedral site

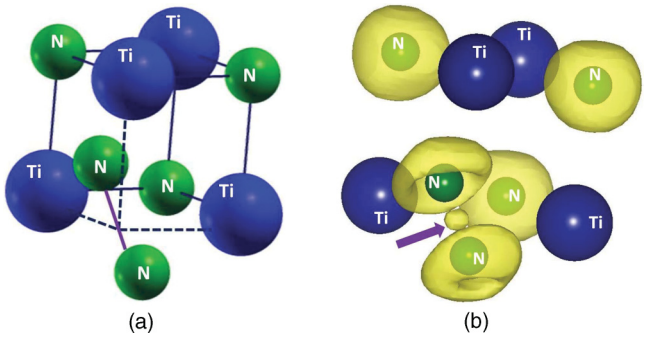

FIG. 2. (Color online) (a)$D_N^N(110)$ configuration. Big (blue) and small (green) spheres are respectively Ti and N atoms. (b) Electron localization function (ELF) values f on a $D_N^N(110)$ defect. Isosurfaces with $f = 0.8$ are shown. The presence of the so-called disynaptic basins (shown with arrow) between neighboring valence shells indicates the formation of a covalent bond between both nitrogen atoms involved in the dumbbell. Drawings produced by VESTA software.[66]

leads to a relaxation of both first and second shells of the surrounded Ti and N atoms. This effect is less important in the case of the I_N defect. The difference of 3.35 eV between I_{Ti} and I_N formation energies can be understood by taking into account that the lattice distortion is larger in the Ti interstitial than in the N interstitial. This can be due to the different radii of these elements as well as the electronic shell polarizability.

The tetrahedral site I_N is not the most stable N interstitial configuration, as already observed by Tsetseris *et al.*[50,57] I_N is less stable by 0.6 eV than the dumbbell $D_N^N(110)$. We have used the electron localization function (ELF) (ELF analysis details can be found in Refs. 67 and 68) to characterize the bonding topology in both I_N and $D_N^N(110)$ defects. ELF values f ranging from 0 to 1 describe very weak ($f = 0$) and very strong ($f = 1$) repulsion between two electrons of the same spin. In the ELF context, a covalent bond appears as isolated isosurfaces between neighboring atoms for large f values (typically more than 0.7). As it can be seen in Fig. 2(b), the split (110) aligned configuration consists in a bonded dimer N-N. The N-N dimer bond length is 1.34 Å, which is in good agreement with calculations from the literature (1.33 Å, Ref. 57). No bond between the N interstitials and the atoms of the TiN matrix have been observed in the case of tetrahedral I_N. As a matter of fact, the energy gain of 0.6 eV can be attributed to a binding energy.

Nevertheless, one must also take into account that the $D_N^N(110)$ induces a smaller distortion of the TiN lattice. This distortion is mainly localized in the (110) plane. The distance between the Ti atom's first shell in this (110) plane and the initial nitrogen site is increased by 0.19 Å and by 0.08 Å in the case of the N second shell. The other atoms are displaced only very slightly (less than 0.03 Å) away for the ideal rocksalt positions.

A slight difference between our results and literature data is observed in the cases of N interstitials. Our obtained values for I_N and $D_N^N(110)$, which are both lower than reported data, could be attributed to the fact that the equilibrium lattice parameter used in this study is higher by 0.02 Å than the reported one. Consequently, the lattice distortion induced by the interstitials here could be less expensive in energy than the one in the studies by Tsetseris.

3. *Mixed divacancies or Schottky defects*

A second class of point defects corresponds to the mixed divacancies, usually named Schottky defects, which consist of the association of a N vacancy and a Ti vacancy. There are several possible geometries of such defects in TiN. The configurations we have studied here are first and second neighboring pairs of Ti and N vacancies. For example, the V_{TiN}(first) and the V_{TiN}(second) configurations consist in the pairing of a N vacancy with a Ti vacancy located in the first neighboring Ti shell (at a distance of 2.13 Å) or in the second neighboring Ti shell (at a distance of 3.69 Å), respectively. Because of the size of this type of defect, calculations were also performed with a 216-atom supercell in order to be sure that no interaction between defects of neighboring supercells introduced some additive errors. As it can be seen in Table II, the formation energies of these defects decrease by about 0.5 eV from the 64-atom to the 216-atom calculation, revealing that some interaction between defects in neighboring supercells probably exists for the 64-atom supercell. Only a very small difference of 40 meV is finally observed between the formation energies of first and second neighboring configurations for the 216-atom cell. Moreover, if one considers the formation energy which is necessary to form the isolated divacancies (i.e., the sum of the corresponding monovacancy formation energies, which is 5.69 eV), one can note that the mixed divacancies V_{TiN}(first) and V_{TiN}(second) seem to be slightly bonded. Indeed, a gain of 0.4 eV is observed when both monovacancies are in the two first coordinance shells. As suggested by Tsetseris *et al.*,[57] migration and clustering of nitrogen and titanium vacancies are largely suppressed except for very high temperature due to the high formation and migration energies as well as repulsive interaction between vacancies (in the case of V_N-V_N and V_{Ti}-V_{Ti}). This result is in good agreement with the mass action law criterion mentioned by Först *et al.*[69] in their study of point defect concentration in metastable Fe-C alloy. It suggests that the very low concentration of single vacancies (due to their high energy of formation) and their low binding energy lead to a very low concentration of the corresponding vacancy cluster. Consequently, aggregated divacancies are not expected to be the dominating species in TiN.

4. *Frenkel pairs*

The formation energies of first neighboring Frenkel pairs, called FP_{Ti}^{first} and FP_N^{first} for Ti and N atoms, respectively, and isolated Frenkel pairs are compared here. In the first neighboring case, the interstitial and the vacancy are located in the same coordinance shell. The interstitial is typically located in the first tetrahedral site near the vacancy site, i.e., at 3.01 Å. In the isolated case, the interstitial and the vacancy are sufficiently far away not to interact and the Frenkel pair is said to be isolated. The recombination of the first neighboring Frenkel pair is observed. It could lead to saying that the recombination radius is larger than 3.01 Å. The formation energies of the isolated Frenkel pairs are 7.34 and 11.56 eV for N and Ti, respectively. As a consequence, isolated Frenkel pairs seem to be unstable in TiN due to the recombination process and their large formation energies.

As a conclusion on point defects stability in TiN, we have shown that monovacancies are the most probable defect. Frenkel pairs are expected to be unstable due to their recombination and their large formation energies because of the interstitial formation values. In the following part, we discuss and give the results obtained on the incorporation of inert gases in TiN and their interaction with point defects such as vacancies which could act as possible traps.

V. INERT GAS INCORPORATION IN TiN

A. Incorporation energy calculation

The incorporation energy of an impurity X, $E_{inc}[X]$, is calculated with the following expression:

$$E_{inc}[X] = E[\text{TiN} + \text{defect} + X] - E[\text{TiN} + \text{defect}] - E[X], \quad (3)$$

TABLE IV. Xe incorporation energies (in eV) in TiN calculated for several interstitials and substitutional configurations in the 64-atom supercell with atomic position relaxation.

I_{Xe}	$I_{Xe}V_N$	$I_{Xe}V_{TiN}$(first)	S^N_{Xe}	$S^N_{Xe}I_N$
23.27	13.55	8.21	13.54	21.61
I_{Xe}[a]	$I_{Xe}V_{Ti}$	$I_{Xe}V_{TiN}$(second)	S^{Ti}_{Xe}	$S^{Ti}_{Xe}I_{Ti}$
21.86	14.16	13.91	15.39	22.97

[a]Value obtained in the 216-atom supercell using both atomic position and volume relaxations.

where E[TiN + defect] is the energy of the impurity-free TiN supercell (containing or not containing a defect) and E[TiN + defect + X] is the energy of the supercell containing the impurity X (containing or not containing a defect). $E[X]$ is the energy per atom of the impurity in its reference state. The incorporation energy requires the knowledge of an arbitrary reference state which has been chosen in the case of rare gas impurities as the ground state of the isolated rare gas in vacuum. Note that in expression (3), the second term corresponds to the crystal which already contains the defect; i.e., the formation energy of the defect is not taken into account here. One can also add to this expression the formation energy of the defect [given by expression (2)] to compare the total energies, usually called the solution energy, which are necessary to form the defect-impurity associations. As mentioned before, the temperature dependence of the formation energy could be taken into account for the nitrogen defects. The nitrogen defect formation was found to vary by 0.15 eV at room temperature due to the temperature contribution. Consequently, the so-called solution energies involving a nitrogen vacancy or a nitrogen interstitial are respectively reduced and increased by 0.15 eV at room temperature in comparison to 0 K.

B. Xe incorporation

Table IV gives the incorporation energies of Xe in several configurations in TiN crystal. Note that the values given in this table correspond to the incorporation energy of the atom of Xe in the already defective TiN crystal [calculated by Eq. (3)]. As an example, if we consider the $I_{Xe}V_N$ configuration and want to take into account the formation energy of the nitrogen monovacancy, the formation energy of the nitrogen monovacancy, i.e., 2.41 eV, has to be added to the 13.55 eV necessary to incorporate Xe in the interstitial site. A comparison of all the incorporation energies is displayed in Fig. 3. The results are described in detail and discussed below.

1. *Xe in tetrahedral position*

Without any single point defect, the more simple interstitial xenon configuration is the tetrahedral position I_{Xe}. This incorporation seems to be largely improbable due to its high energy cost, which is higher than 20 eV. Indeed, due to its large atomic radius, the interstitial Xe atom induces a very large distortion of the host lattice. In this configuration, the atomic displacement of the first shell, δR_{first}, is about 0.46 and 0.53 Å for N and Ti atoms, respectively, as mentioned in Table V.

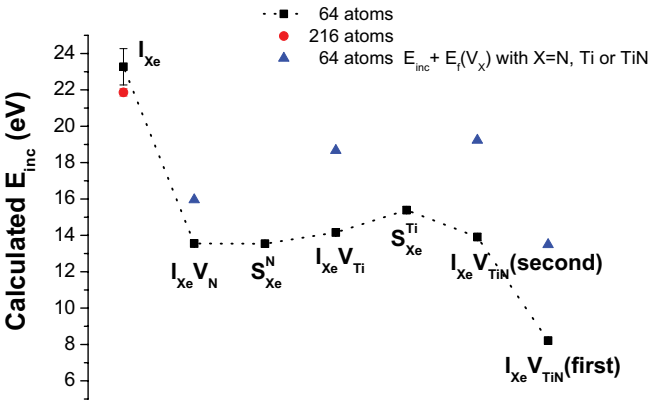

FIG. 3. (Color online) Xe incorporation energies in TiN calculated for several interstitials and substitutional configurations in the 64-atom supercell with atomic position relaxation. Values which take into account the defect formation energy at 0 K are also given (blue triangles).

2. *Xe in tetrahedral position associated with monovacancies*

Xe incorporation in a tetrahedral position in the vicinity of a single vacancy ($I_{Xe}V_N$ and $I_{Xe}V_{Ti}$) was calculated. To associate Xe in the interstitial position with a single vacancy in the first neighboring shell permits a considerable reduction of 9.72 and 9.11 eV in incorporation energy considering respectively the nitrogen ($I_{Xe}V_N$) and the titanium vacancies ($I_{Xe}V_{Ti}$). In these configurations, the xenon atom relaxes from the interstitial position into the vacancy sites (at the N site for the N vacancy and at 0.04 Å from the Ti site for the Ti vacancy). This phenomenon reduces the host lattice distortion as mentioned in Table V. This effect is more important in the case of the nitrogen vacancy and could explain the gain difference being larger by 0.61 eV for the nitrogen vacancy than the titanium vacancy.

3. *Xe in substitution of Ti/N atom*

Xe substituting an atom of the TiN crystal (S^{Ti}_{Xe} and S^N_{Xe}) has been studied. Indeed, the fact that the xenon atom relaxes to the single vacancy site tends to suggest that the substitutional incorporation may be more stable than tetrahedral incorporation. When the xenon atom substitutes a nitrogen atom (S^N_{Xe}), this assumption seems to be true as both incorporation energies of S^N_{Xe} and $I_{Xe}V_N$ configurations are the same. Nevertheless, when xenon substitutes a titanium atom (S^{Ti}_{Xe}), the incorporation energy is reduced by 1.23 eV in comparison to the $I_{Xe}V_{Ti}$ configuration. As a consequence,

TABLE V. Atomic displacements of the first shell(s), δR, due to the presence of the inert gas incorporation in TiN. Positive values indicate an increase of the interatomic distances.

δR_{first} (Å)	I_{gas}	$I_{gas}V_N$	$I_{gas}V_{Ti}$
He	+0.11 (N)/ +0.13 (Ti)	+0.20 (Ti)	+0.09 (N)
Ne	+0.23 (N)/ + 0.26 (Ti)	+0.26 (Ti)	+0.14 (N)
Ar	+0.35 (N)/ +0.36 (Ti)	+0.30 (Ti)	+0.26 (N)
Kr	+0.39 (N)/ +0.43 (Ti)	+0.32 (Ti)	+0.43 (N)
Xe	+0.46 (N)/ +0.53 (Ti)	+0.34 (Ti)	+0.49 (N)

Xe incorporation in the nitrogen site is more stable than in the titanium site. This is probably due to the effective charge of the neighboring first shell, which could be considered positive in the N site (due to the neighboring Ti atoms) and negative in the Ti site (due to the neighboring N atoms).

4. Xe in tetrahedral position associated with mixed divacancies

We have also studied the xenon interstitial association with mixed divacancies [$I_{Xe}V_{TiN}$(first) and $I_{Xe}V_{TiN}$(second)]. In these cases, a big difference appears compared to the previous associations. If the two vacancies are second neighbors [$I_{Xe}V_{TiN}$(second)], the gain in energy is about 9.36 eV compared to the interstitial incorporation in the perfect crystal. Indeed, in this case, the xenon atom stays in the tetrahedral position and the host distortion is partially compensated by the N and Ti vacancies. If the vacancies are first neighbors [$I_{Xe}V_{TiN}$(first)], the xenon atom position relaxes to the center (equal distance) between the two vacancies. This phenomenon induced a large gain of 15.06 eV in energy due to the smaller distortion of the host lattice. Nevertheless, due to the size of this type of defect, calculations would probably need to be performed with a 216-atom supercell ensuring the reduction of interactions between defects of neighboring supercells and energetics bias.

Moreover, taking into account the vacancy formation energy reveals that first forming vacancies and then incorporating the Xe atom is less expensive than introducing a Xe atom in a perfect lattice (see Fig. 3). These energy gains could be interpreted as trapping energy. As a consequence, Xe is trapped in a vacancy. More probably, Xe could be easily involved in vacancy-Xe coprecipitation. This phenomenon is in good agreement with experimental studies which have shown that Xe has a very low solubility in TiN and has the tendency to form bubbles at low concentration (less than 0.4 at. %).[38,43]

5. Xe in tetrahedral site and Ti/N interstitial exchange

We have also considered the exchange between a Xe atom in a tetrahedral crystalline position and one atom of the lattice. This configuration could correspond to a xenon atom that knocks an atom (N or Ti) out of its lattice position and the latter comes to the interstitial tetrahedral position ($S^{N}_{Xe}I_N$ and $S^{Ti}_{Xe}I_{Ti}$, respectively). This phenomenon could happen, as an example, during the irradiation process because Xe is introduced with a certain energy in the material and can produce atomic displacements. To simulate this situation, the previous incorporation of a Xe atom in substitution was coupled with a self-interstitial in the tetrahedral position ($S^{N}_{Xe}I_N$ and $S^{Ti}_{Xe}I_{Ti}$ for N and Ti atoms, respectively). The exchange configuration decreases partly the large stress induced by lattice distortion and releases about 1.66 and 0.30 eV considering nitrogen and titanium interstitials, respectively. The difference between nitrogen and titanium as interstitials in this case is consistent with the existing difference observed with the same interstitials in the perfect TiN lattice (cf. Table II). This phenomenon was already observed by Tsetseris *et al.*[44] in the case of Ar incorporation associated with nitrogen interstitials. It was interpreted by these authors as a trapping of a nitrogen atom by the rare gas and the energy release was considered a binding energy.

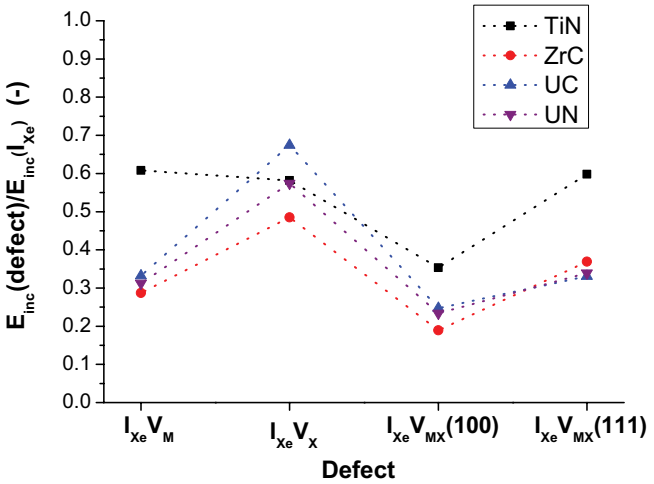

FIG. 4. (Color online) Xe incorporation energy trends in TiN (this study), UC,[70] UN,[71] ZrC,[72] and 3C-SiC (Ref. 73) obtained using the same calculation approach. Values are divided by the corresponding interstitial incorporation energy for the sake of trend clarity.

6. Comparison with first-principles results in structurelike materials

The study of the incorporation of xenon in UC,[70] UN,[71] ZrC,[72] and 3C-SiC (Ref. 73) can be found in the literature. We compare here the incorporation energies and the solution energies obtained using the same calculation approach in order to find trends for some structurelike materials. Similar results for the location of xenon in crystal have been obtained for all of these materials, as can be seen in Fig. 4. Indeed, for all investigated materials, the xenon incorporation energies at first neighboring mixed divacancies ($I_{Xe}V_{MX}$(first) with M = Si, Ti, Zr, or U, and X = C or N) were the lowest. This phenomenon is probably the consequence of a steric effect as the incorporation energy of xenon decreases with the increase of the vacancy volume, i.e., the volume which was previously occupied by the considered atom.

To summarize, xenon incorporation is largely facilitated by the presence of vacancies and xenon is probably trapped by them. This is probably a consequence of the large stress induced in the host lattice by Xe incorporation. Indeed, vacancies reduce the stress induced by the presence of the large Xe atom and consequently the energy cost of its incorporation. The larger the vacancy site is, the lower the stress is. Experimentally, this phenomenon could be responsible for the generally low solubility of Xe in materials and its precipitation into gas bubbles.

C. Other inert gas incorporation

Let us now present the results on the incorporation of other inert gas atoms, He, Ne, Ar, and Kr, in the TiN crystal. We performed similar calculations for these rare gases incorporated in the tetrahedral interstitial positions into the perfect TiN crystal (I_{gas}) and into the lattice with monovacancy ($I_{gas}V_N$ and $I_{gas}V_{Ti}$). These results are given in Table VI.

As it can be observed, the tetrahedral position is the least favored site of incorporation whatever the considered rare gas.

TABLE VI. Inert gas incorporation energies (in eV) in TiN calculated for several interstitial configurations in the 64-atom supercell with atomic position relaxation.

Rare gas	I_{gas}	$I_{gas}V_N$	$I_{gas}V_{Ti}$
He	4.70	3.23	1.13
Ne	9.22	4.92	3.08
Ar	15.41	7.92	8.64
Kr	18.58	9.85	11.23

This instability seems to be proportional to the atomic radius of the inert gas as shown in Fig. 5. This phenomenon is probably the consequence of the host lattice deformation in the presence of the interstitial atom as mentioned previously (see Table V). The stress induced by inert gas incorporation can be partly reduced when the inert gas is trapped at a vacancy site as already observed for the xenon atom. The release energy in the case of the Kr atom is, as an example, about 8.73 and 7.35 eV for nitrogen and titanium vacancy sites, respectively. The most favored vacancy site is the nitrogen site for Ar, Kr, and Xe. In the case of He and Ne atoms, it is the titanium vacancy site. This phenomenon is not yet well understood. It could be due to the van der Waals effect of the long-range interaction, which is not well described by the DFT in the generalized gradient approximation (GGA). This effect, which has a dominant contribution in the chemical interaction involving rare gas elements, is expected to be more important for the lightest (He) than for the heaviest (Xe) atom as a consequence of the largest polarizability of the heaviest atoms.[74] The so-called DFT-D2 Grimme approach,[75] which consists in adding a semiempirical dispersion potential to the conventional Kohn-Sham DFT energy and the van der Waals density functional (vdW-DF) approach[76] which considers the nonlocal interaction as a density-density interaction, are available in the recent release of the VASP code (version 5.2) in order to estimate the van der Waals interactions in a solid. An earlier version of VASP is used in this study, so the van der Waals contributions could not be estimated precisely. At the phenomenological level, in a UO_2 crystal, Gryaznov *et al.*[77] mentioned a van der Waals contribution of −0.25 eV to the He incorporation energy, taking into account *a posteriori* shell-model empirical potentials. Moreover, Bertolus *et al.*[74] showed that, for the incorporation of rare gases in small molecules such as HeHCN and KrHCN, a relative error of several percent was found on their binding energy. In our case, the incorporation energies of helium are about several eV with a minimum of 1.13 eV for the $I_{He}V_{Ti}$ case. Assuming the same order of magnitude as Gryaznov *et al.*,[77] the relative errors in incorporation energies are expected to be about 10% for $I_{He}V_N$ and I_{He}, and about 25% for $I_{He}V_{Ti}$. Nevertheless, the results presented here give reliable trends for the incorporation energies of rare gases in TiN.

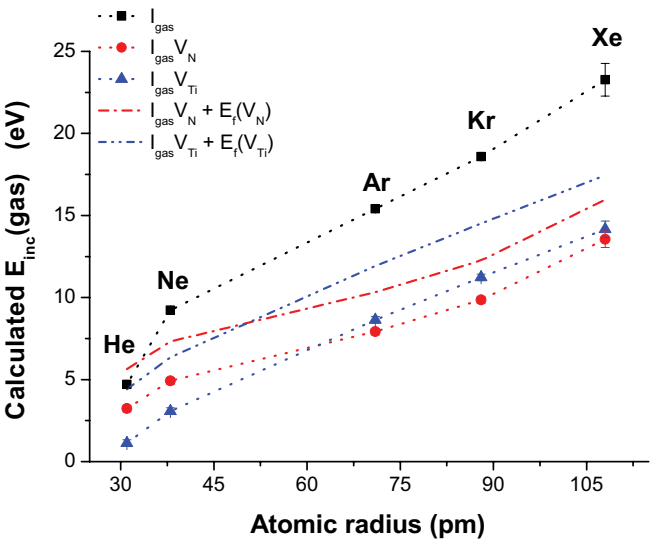

FIG. 5. (Color online) Comparison of inert gas incorporation energies in TiN calculated for several interstitial configurations in the 64-atom supercell with atomic position relaxation. Values which take into account the defect formation energy at 0 K are also given.

As a partial conclusion, we have shown that the incorporation energies of inert gases follow the trends of the site that reduces the lattice stress. This site is generally the larger site available. These sites are vacancies and act as traps for rare gases with a non-negligible trapping energy. However, all the incorporation energies are positive, which indicates that inert gases are not stabilized in TiN. Consequently, the propensity to form bubbles or to aggregate is important. Concerning the Xe atoms, these results are consistent with experimental data that have shown bubble formation at low Xe concentration (about 0.4 at. %) after high-temperature annealing.[43]

VI. CONCLUSION

The current work has used DFT calculations to determine the most favored incorporation site of rare gases (from helium to xenon), with a focus on xenon, in titanium nitride. The DFT-GGA method has been used to calculate the formation energy of several point defects (vacancies, interstitials, divacancies, Frenkel pairs) and then the incorporation energy of rare gases in these defects. The main results show that the incorporation energies of rare gases follow the trend of the larger sites available, which generally present the most reduced lattice stress. These sites are vacancies and, in the case of Xe atoms, the Schottky defect with vacancies located at the edge of the cubic lattice. Vacancy defects act as traps for rare gases with a non-negligible trapping energy. Comparison with several carbides and nitrides with the same rocksalt structure has revealed that the steric effect is probably the most important effect, which affects the xenon behavior in materials such as its propensity to aggregate and then form bubbles.

*Present address: rene.bes@cnrs-orleans.fr
†yves.pipon@ipnl.in2p3.fr

[1]J. E. Sundgren and H. T. G. Hentzell, J. Vac. Sci. Technol. A **4**, 2259 (1986).
[2]H. E. Rebenne and D. G. Bhat, Surf. Coat. Technol. **63**, 1 (1994).
[3]S. Niyomsoan, W. Grant, D. L. Olson, and B. Mishra, Thin Solid Films **415**, 187 (2002).
[4]J. M. Lackner, Vacuum **78**, 73 (2005).

[5]P. J. Martin, R. P. Netterfield, W. G. Sainty, and C. G. Pacey, J. Vac. Sci. Technol. A **2**, 341 (1984).

[6]Y. Claesson, M. Georgson, A. Roos, and C.-G. Ribbing, Sol. Energy Mat. **20**, 455 (1990).

[7]K. E. Andersson, M. K. Wahlström, and A. Roos, Thin Solid Films **214**, 213 (1992).

[8]R. Gordon, J. Non-Cryst. Solids **218**, 81 (1997).

[9]G. B. Smith, A. Ben-David, and P. D. Swift, Renewable Energy **22**, 79 (2001).

[10]K. Bewilogua, G. Bräuer, A. Dietz, J. Gäbler, G. Goch, B. Karpuschewski, and B. Szyszka, CIRP Ann. **58**, 608 (2009).

[11]J. Kohlscheen, H.-R. Stock, and P. Mayr, Surf. Coat. Technol. **120-121**, 740 (1999).

[12]Z. Peng, H. Miao, W. Wang, S. Yang, C. Liu, and L. Qi, Surf. Coat. Technol. **166**, 183 (2003).

[13]Z. Peng, H. Miao, L. Qi, W. Wang, S. Yang, and C. Liu, Acta Mater. **51**, 3085 (2003).

[14]J. Musil, Surf. Coat. Technol. **125**, 322 (2000).

[15]S. Hao, B. Delley, S. Veprek, and C. Stampfl, Phys. Rev. Lett. **97**, 086102 (2006).

[16]S. W. Wang, R. Gudipati, A. S. Rao, T. J. Bostelmann, and Y. G. Shen, Appl. Phys. Lett. **91**, 081916 (2007).

[17]J. G. Steele, J. F. McCabe, and I. E. Barnes, J. Dent. (Oxford, UK) **19**, 226 (1991).

[18]P. R. Mezger and N. H. J. Creugers, J. Dent. (Oxford, UK) **20**, 342 (1992).

[19]K. H. Chung, G. T. Liu, J. G. Duh, and J. H. Wang, Surf. Coat. Technol. **188-189**, 745 (2004).

[20]A. Shenhar, I. Gotman, S. Radin, P. Ducheyne, and E. Y. Gutmanas, Surf. Coat. Technol. **126**, 210 (2000).

[21]A. P. Serro, C. Completo, R. Colaço, F. dos Santos, C. Lobato da Silva, J. M. S. Cabral, H. Araújo, E. Pires, and B. Saramago, Surf. Coat. Technol. **203**, 3701 (2009).

[22]B. Subramanian, C. V. Muraleedharan, R. Ananthakumar, and M. Jayachandran, Surf. Coat. Technol. **205**, 5014 (2011).

[23]V.-H. Pham, S.-H. Jun, H.-E. Kim, and Y.-H. Koh, Appl. Surf. Sci. **258**, 2864 (2012).

[24]M. Wittmer, B. Studer, and H. Melchior, J. Appl. Phys. **52**, 5722 (1981).

[25]C. Ernsberger, J. Nickerson, A. Miller, and D. Banks, J. Vac. Sci. Technol. A **3**, 2303 (1985).

[26]M. Mändl, H. Hoffmann, and P. Kücher, J. Appl. Phys. **68**, 2127 (1990).

[27]K.-C. Park, K.-B. Kim, I. J. M. M. Raaijmakers, and K. Ngan, J. Appl. Phys. **80**, 5674 (1996).

[28]M. J. Madou, *Fundamentals of Microfabrication: The Science of Miniaturization*, 2nd ed. (CRC Press, New York, 2002), p. 615.

[29]M. Moriyama, T. Kawazoe, M. Tanaka, and M. Murakami, Thin Solid Films **416**, 136 (2002).

[30]H. C. Chen, B. H. Tseng, M. P. Houng, and Y. H. Wang, Thin Solid Films **445**, 112 (2003).

[31]L. Gao, J. Gstöttner, R. Emling, M. Balden, C. Linsmeier, A. Wiltner, W. Hansh, and D. Schmitt-Landsiedel, Microelectron. Eng. **76**, 76 (2004).

[32]Y.-H. Shin and Y. Shimogaki, Sci. Technol. Adv. Mat. **5**, 399 (2004).

[33]W. E. Martinez, G. Gregori, and T. Mates, Thin Solid Films **518**, 2585 (2010).

[34]L. Hultman, Vacuum **57**, 1 (2000), and references therein.

[35]GenIV Technology Roadmap, [http://www.gen-4.org], 2002.

[36]*Les réacteurs nucléaires à caloporteurs gaz*, monograph (DEN, 2006).

[37]H. O. Pierson, *Handbook of Refractory Carbides and Nitrides* (Noyes Publications, Park Ridge, NJ, 1996).

[38]T. Weber, W. Bolse, and K. Lieb, Nucl. Instrum. Methods: Phys. Res. B **50**, 95 (1990).

[39]A. J. Perry, V. Vavolda, D. Rafaja, D. L. Williamson, and B. D. Sartwell, Surf. Coat. Technol. **54-55**, 180 (1992).

[40]S. Gavarini, N. Toulhoat, C. Peaucelle, P. Martin, J. Mende, Y. Pipon, and H. Jaffrezic, J. Nucl. Mater. **362**, 364 (2007).

[41]R. Bès, N. Millard-Pinard, S. Gavarini, S. Cardinal, V. Garnier, H. Khodja, A. Malchère, P. Martin, and C. Peaucelle, Nucl. Instrum. Methods: Phys. Res. B **268**, 1880 (2010).

[42]S. Gavarini, R. Bès, N. Millard-Pinard, S. Cardinal, C. Peaucelle, A. Perrat-Mabilon, V. Garnier, and C. Gaillard, J. Appl. Phys. **109**, 014906 (2011).

[43]R. Bès, C. Gaillard, N. Millard-Pinard, S. Gavarini, P. Martin, S. Cardinal, C. Esnouf, A. Malchère, and A. Perrat-Mabilon J. Nucl. Mater. **434**, 56 (2013).

[44]L. Tsetseris, N. Kalfagiannis, S. Logothetidis, and S. T. Pantelides, Phys. Rev. B **78**, 094111 (2008).

[45]P. E. Blöchl, Phys. Rev. B **50**, 17953 (1994).

[46]G. Kresse and D. Joubert, Phys. Rev. B **59**, 1758 (1999).

[47]Y. Wang and J. P. Perdew, Phys. Rev. B **43**, 8911 (1991).

[48]H. J. Monkhorst and J. D. Pack, Phys. Rev. B **13**, 5188 (1976).

[49]F. Birch, Phys. Rev. **71**, 809 (1947).

[50]L. Tsetseris, N. Kalfagiannis, S. Logothetidis, and S. T. Pantelides, Phys. Rev. Lett. **99**, 125503 (2007).

[51]S. S. Carara, L. A. Thesing, and P. Piquini, Thin Solid Films **515**, 2730 (2006).

[52]S. V. Dudiy and B. I. Lundqvist, Phys. Rev. B **64**, 045403 (2001).

[53]M. Marlo and V. Milman, Phys. Rev. B **62**, 2899 (2000).

[54]D. R. Lide, *CRC Handbook of Chemistry and Physics*, 91st ed. (CRC Press, Boca Raton, FL, 2011).

[55]M. Guemmaz, G. Moraitis, A. Mosser, M. A. Khan, and J.-C. Parlebas, J. Alloys Compd. **262-263**, 397 (1997).

[56]M. Guemmaz, A. Mosser, and J.-C. Parlebas, J. Electron Spectrosc. Relat. Phenom. **107**, 91 (2000).

[57]L. Tsetseris, N. Kalfagiannis, S. Logothetidis, and S. T. Pantelides, Phys. Rev. B **76**, 224107 (2007).

[58]R. Evarestov, E. Blokhin, D. Gryaznov, E. A. Kotomin, R. Merkle, and J. Maier, Phys. Rev. B **85**, 174303 (2012).

[59]Y. A. Mastrikov, E. Heifets, E. A. Kotomin, and J. Maier, Surf. Sci. **603**, 326 (2009).

[60]K. Johnston, M. R. Castell, A. T. Paxton, and M. W. Finnis, Phys. Rev. B **70**, 085415 (2004).

[61]E. Heifets, S. Piskunov, E. A. Kotomin, Y. F. Zhukovskii, and D. E. Ellis, Phys. Rev. B **75**, 115417 (2007).

[62]E. Heifets, J. Ho, and B. Merinov, Phys. Rev. B **75**, 155431 (2007).

[63]M. W. Chase, J. Phys. Chem. Ref. Data, Monogr. **9**, 1621 (1998).

[64]S.-H. Jhi, S. G. Louie, M. L. Cohen, and J. Ihm, Phys. Rev. Lett. **86**, 3348 (2001).

[65]S.-H. Jhi, S. G. Louie, M. L. Cohen, and J. W. Morris, Phys. Rev. Lett. **87**, 075503 (2001).

[66]K. Momma and F. Izumi, J. Appl. Crystallogr. **44**, 1272 (2011).

[67]B. Silvi and A. Savin, Nature (London) **371**, 683 (1994).

[68]B. Silvi and C. Gatti, J. Phys. Chem. A **104**, 947 (2000).

[69]C. J. Forst, J. Slycke, K. J. Van Vliet, and S. Yip, Phys. Rev. Lett. **96**, 175501 (2006).
[70]M. Freyss, Phys. Rev. B **81**, 014101 (2010).
[71]M. Klipfel and P. Van Uffelen, J. Nucl. Mater. **422**, 137 (2012).
[72]Y. Pipon (private communication).
[73]M. Bertolus, http://tel.archives-ouvertes.fr/tel-00665253 (unpublished).
[74]M. Bertolus, M. Major, and V. Brenner, Phys. Chem. Chem. Phys. **14**, 553 (2012).
[75]S. Grimme, J. Comput. Chem. **27**, 1787 (2006).
[76]M. Dion, H. Rydberg, E. Schroder, D. C. Langreth, and B. I. Lundqvist, Phys. Rev. Lett. **92**, 246401 (2004).
[77]D. Gryaznov, E. Heifets, and E. Kotomin, Phys. Chem. Chem. Phys. **11**, 7241 (2009).